Hydrodynamic Model Description
Hellisay, Isle of Barra, CAR/L/1095612

June 2022

› Mowi Scotland

[redacted]

CONTENTS

LIST OF FIGURES

LIST OF TABLES

1. Model Description

The hydrodynamic model used in the Hellisay Azamethiphos Dispersion Modelling (Mowi Scotland Ltd., 2022) was RiCOM (River and Coastal Ocean Model), a general-purpose hydrodynamics and transport model, which solves the standard Reynolds-averaged Navier-Stokes equation (RANS) and the incompressibility condition, applying the hydrostatic and Boussinesq approximations. It has been tested on a variety of benchmarks against both analytical and experimental data sets (e.g. Walters & Casulli 1998; Walters 2005a, b). The model has been previously used to investigate the inundation risk from tsunamis and storm surge on the New Zealand coastline (Walters 2005a; Gillibrand et al. 2011; Lane et al. 2011), to study tidal currents in high energy tidal environments (Walters et al. 2010) and, more recently, to study tidal energy resource (Plew & Stevens 2013; Walters et al. 2013; Walters 2016) and the effects of energy extraction on the ambient environment (McIlvenny et al. 2016; Gillibrand et al. 2016).

The basic equations considered here are the three-dimensional (3D) shallow water equations, derived from the Reynolds-averaged Navier-Stokes equations by using the hydrostatic assumption and the Boussinesq approximation. The continuity equation for incompressible flows is:

$$\nabla \cdot u + \frac{\partial w}{\partial z} = 0 \tag{1}$$

where **u**(x,y,z,t) is the horizontal velocity vector, w(x,y,z,t) is the vertical velocity, ∇ is the horizontal gradient operator, and z is the vertical coordinate. The momentum equation in non-conservative form is given by:

$$\frac{Du}{Dt} + f\hat{z} \times u + \frac{1}{\rho_0}\nabla p - \frac{\partial}{\partial z}\left(A_V \frac{\partial u}{\partial z}\right) - \nabla \cdot (A_h \nabla u) + F = 0 \tag{2}$$

where t is time; f(x,y) is the Coriolis parameter; $\hat{\mathbf{z}}$ is the upward unit vector; p(x,y,z,t) is pressure; ρ_0 is a reference density; A_V(x,y,z,t) and A_h(x,y,z,t) are the vertical and horizontal eddy viscosities respectively; **F** represents body forces including form drag from obstacles in the flow; and x, y are the horizontal coordinates aligned to the east and north respectively.

The free surface equation is formed by vertically integrating the continuity equation and applying the kinematic free surface and bottom boundary conditions:

$$\frac{\partial \eta}{\partial t} - \nabla \cdot \left(\int_{-H}^{\eta} u dz\right) = 0 \tag{3}$$

where H is the water depth relative to the mean level of the sea.

The model can be run in two- or three-dimensional mode. Frictional stress, $\boldsymbol{\tau}_b$, is applied at the seabed as a quadratic function of velocity:

$$\tau_b = \rho C_D U_b |U_b| \tag{4}$$

where ρ = 1025 kg m^{-3} is the water density. The velocity, U_b, is either the velocity at the lowest sigma layer if the model is run in 3D or the depth-averaged velocity if run in 2D. The drag coefficient, C_D, can be either a constant or calculated from the bed roughness lengthscale, z_0, using:

$$C_D = \left(\frac{\kappa}{\ln\left((z_b+z_0)/z_0\right)}\right)^2 \quad (5)$$

where κ=0.4 is von Karman's constant, and z_b is the height above the bed of the lowest velocity point.

Wind forcing was applied as a surface stress calculated from hourly wind speed and direction. Wind stress was calculated from the wind velocity by a standard quadratic relation:

$$\tau_x = \rho_a C_S u W \quad (6a)$$
$$\tau_y = \rho_a C_S v W \quad (6b)$$

where (u,v) are the East and North components of wind velocity respectively, W is the wind speed ($W = [u^2+v^2]^{½}$), ρ_a is the density of air, and the surface drag coefficient C_S is calculated following Wu (1982) or Large and Pond (1981).

The equations are discretized on an unstructured grid of triangular elements which permits greater resolution of complex coastlines. The momentum and free surface equations are solved using semi-implicit techniques to optimize solution time and avoid the CFL stability constraint (Walters 2016). The material derivative in (2) is discretized using semi-Lagrangian methods to remove stability constraints on advection (Casulli, 1987; Walters et al. 2008). The Coriolis term is solved using a 3rd order Adams-Bashforth method (Walters et al. 2009). Full details of the model discretization and solution methods can be found in Walters et al. (2013) and Walters (2016). The solution methods provide a fast, accurate and robust code that runs efficiently on multi-core desktop workstations with shared memory using OpenMP. Full details of the model discretization and solution methods, including the basis of the application to tidal energy, are given by Walters et al. (2013) and Walters (2016).

2. Configuration and Boundary Forcing for Hellisay

The unstructured mesh used in the modelling (Figure 1) was adapted from the East Coast of Lewis and Harris (ECLH) sub-model mesh of the Scottish Shelf Model (SSM; MS, 2016). The model resolution was enhanced in the South Uist region, particularly around the Mowi site at Hellisay (Figure 2). The spatial resolution of the model varied from 20m in some inshore waters and round the farm pens to 5km along the open boundary. The model consisted of 75,790 nodes and 143,144 triangular elements. The model was run in 2D mode.

Regional bathymetry was taken from the EMODnet digital terrain model (https://emodnet.ec.europa.eu/en/bathymetry). These data were supplemented by a local multibeam bathymetry survey around the site undertaken in April 2019 (Figure 3). The combined bathymetry model (Figure 3) merges the detailed bathymetry on the high-resolution mesh around the site with the regional bathymetry in the surrounding area.

The model is forced at the outer boundaries by 8 tidal constituents (M_2, S_2, N_2, K_2, O_1, K_1, P_1 and Q_1) which were derived from tidal analysis (Pawlowicz et al., 2002) of the sea surface elevations at the closest nodes from the Scottish Shelf Model climatology (Marine Scotland, 2016). Spatially- and temporally-varying wind speed and direction data are taken from the ERA5 global reanalysis dataset (ECMWF, 2021) for the required simulation periods.

Figure 1. The ECLH mesh and domain of the modelling study (SSM)

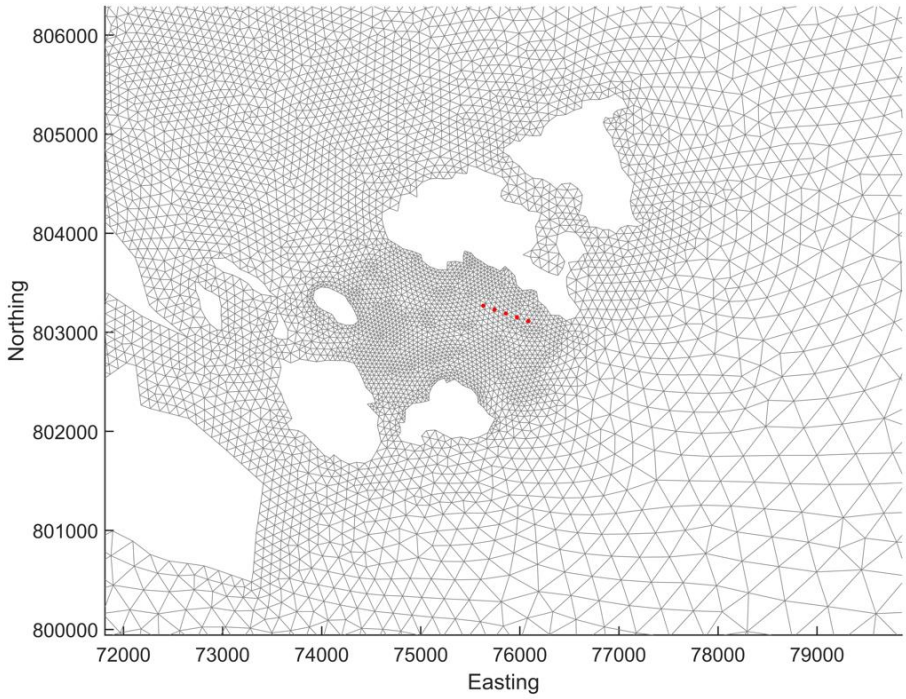

Figure 2. The unstructured mesh around the Hellisay site in the modified model grid, with the proposed cage locations indicated (•).

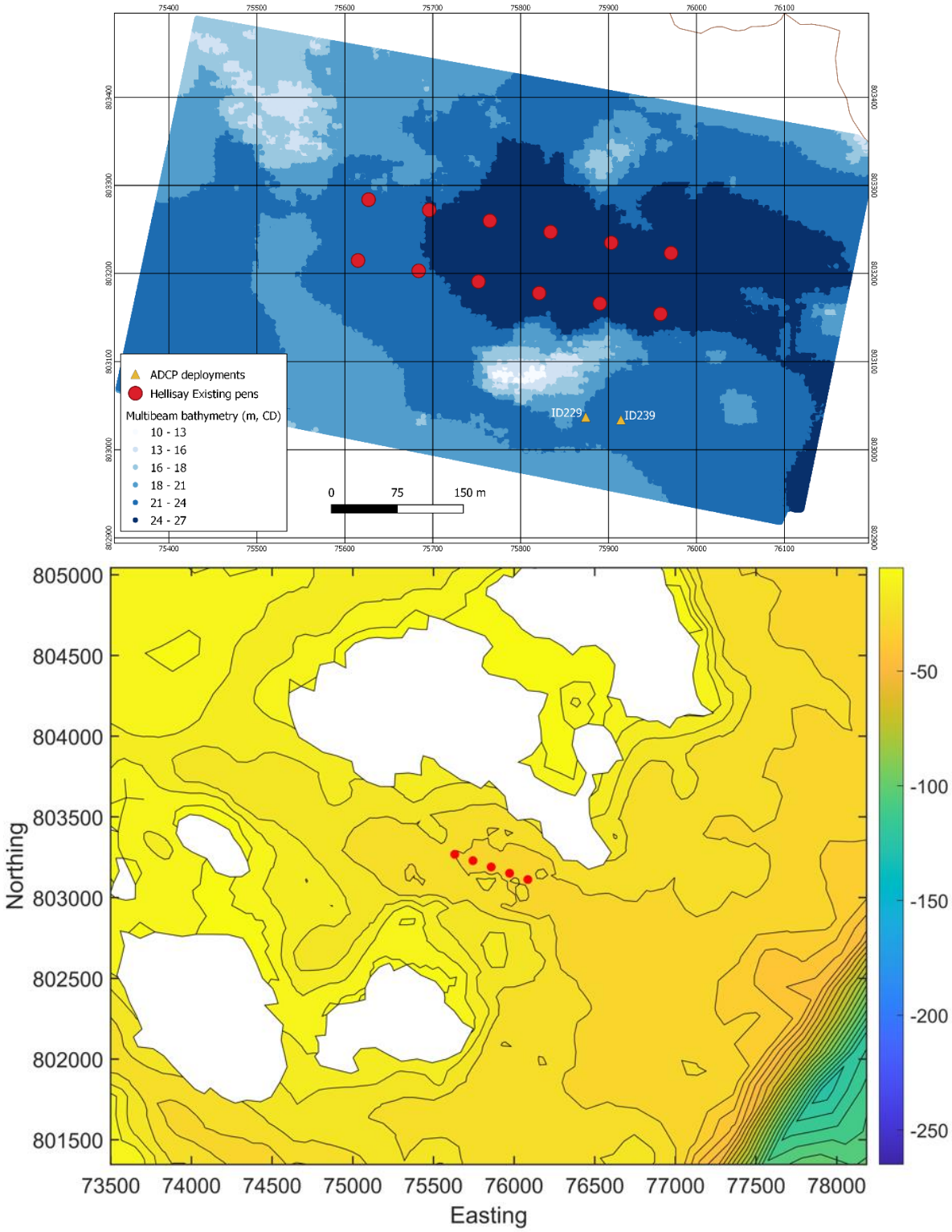

Figure 3. Water depths (m) from a multibeam survey around the Hellisay site (top) with the existing pen locations shown (●); Model bathymetry (m) in the area around Hellisay salmon farm (bottom) with the proposed pen locations (●).

3. Model Calibration and Validation

The RiCOM model has previously been calibrated against sea level and current meter data from the north of Scotland (Gillibrand et al. 2016). For the current study, the model was further calibrated against hydrographic data collected in the region of the farm site in 2018. The data are described in the relevant hydrographic reports. In June 2018, an Acoustic Doppler Current Profiler (ADCP) was deployed close to the farm site (Figure 4) until August 2018 (ID229). In August 2018, another ADCP was deployed close to the farm site (Figure 4) until October 2018 (ID239). In all, 126 days of current data were used in this application. ADCP deployments provided both current velocity and seabed pressure data, which were used to calibrate and validate modelled velocity and sea surface height. The model was calibrated initially against data from June – August 2018 (ID229), then validated against data from the other deployment, ID239.

For each simulation, the model was "spun-up" for three days with boundary forcing ramped up from zero over a period of 48 hours. The model state at the end of the 72-hour spin-up period was stored, and the main simulations "hot-started" from this state.

The following main simulations were performed, corresponding with the dates of the ADCP deployments:

(i) Calibration: 7th June 2018 – 13th August 2018 (ID229)
(ii) Validation: 13th August 2018 – 30th October 2018 (ID239)

[Note that the dates above refer to the main simulations and that the spin-up simulations ran for three days prior to the start dates given above.]

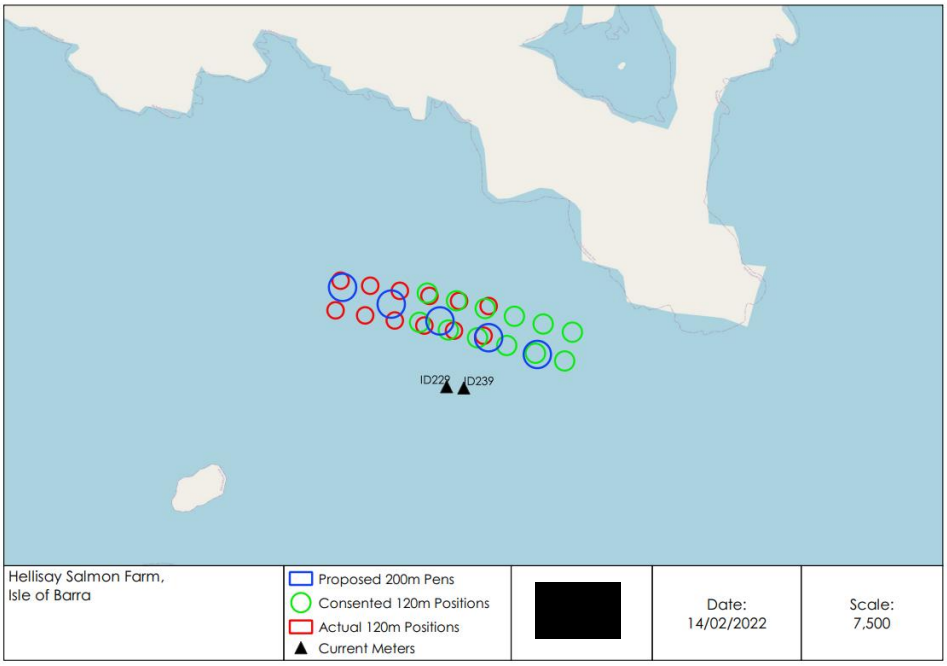

Figure 4. Locations of the ADCP deployments relative to the existing, consented and proposed pens at the Hellisay site.

Model performance is assessed using three metrics: the mean absolute error (MAE), the root-mean-square error (RMSE) and the model skill (d_2). The first two are standard measures of model accuracy; the third, d_2, is taken from Willmott et al. (1985) and lies in the range $0 \leq d_2 \leq 1$, with $d_2 = 0$ implying zero model skill and $d_2 = 1$ indicating perfect skill.

3.1 Calibration: June – August 2018, ID229

The calibration used observed depth and current velocity from the ADCP location to compare with modelled sea surface height (SSH) and velocity (ADCP deployment ID229). The model was calibrated by varying the value of the drag coefficient, C_D, in Equation A4, which determines the frictional effect of the seabed on the flow. Simulations were performed with a range of values of C_D, varying over the range $0.002 \leq C_D \leq 0.02$. After a number of simulations, a final parameter set was selected (Table 1).

Table 1. Parameter values chosen for the RiCOM model during the calibration simulations.

Parameter Description	Value
Drag coefficient, C_D	0.02
Number of vertical levels	1
Model time step (s)	72

The results of the calibration exercise are presented in Figure 5 – Figure 8 and Table 2. At the ADCP location, the sea surface height was reasonably accurately modelled, with model skill of 0.99. The mean absolute error (MAE) and root-mean-square error (RMSE) values of 0.14 m and 0.17m are about 3.3% and 4% of the spring tide range (4.28m) respectively.

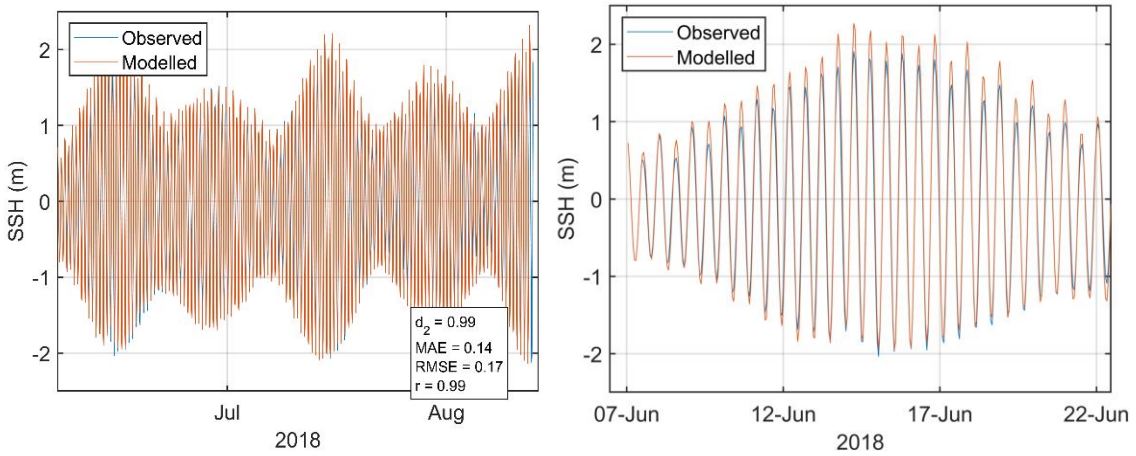

Figure 5. Comparison between observed and modelled sea surface height from June – August 2018 (ADCP deployment ID229) using model parameter values from Table 1. Both the full record (left) and a subset of 15 days (right) are shown. Observed data are in blue, model results in red.

For the calibration period, the model skill scores were 0.52 and 0.41 for the East and North components of velocity respectively. RMSE values were 0.08 and 0.05 respectively (Table 2). The scatter plots and histograms demonstrate that the modelled current had broadly the same

magnitude and direction characteristics as the observed data (Figure 7 and Figure 8), although the prevailing modelled current orientation is offset slightly relative to the orientation of the observed currents (Figure 7). This may be related to the small shoaling bank to the west of the ADCP deployment location (Figure 3) which may have acted as a obstacle to the prevailing flow, causing a deviation in the flow direction.

Table 2. Model performance statistics for sea surface height (SSH) and East and North velocity at the ADCP location from June – August 2018 (ID229).

	SSH	East	North
Model skill, d_2	0.99	0.52	0.41
Mean Absolute Error (MAE)	0.14 m	0.07 m s^{-1}	0.04 m s^{-1}
Root-Mean-Square Error (RMSE)	0.17 m	0.08 m s^{-1}	0.05 m s^{-1}

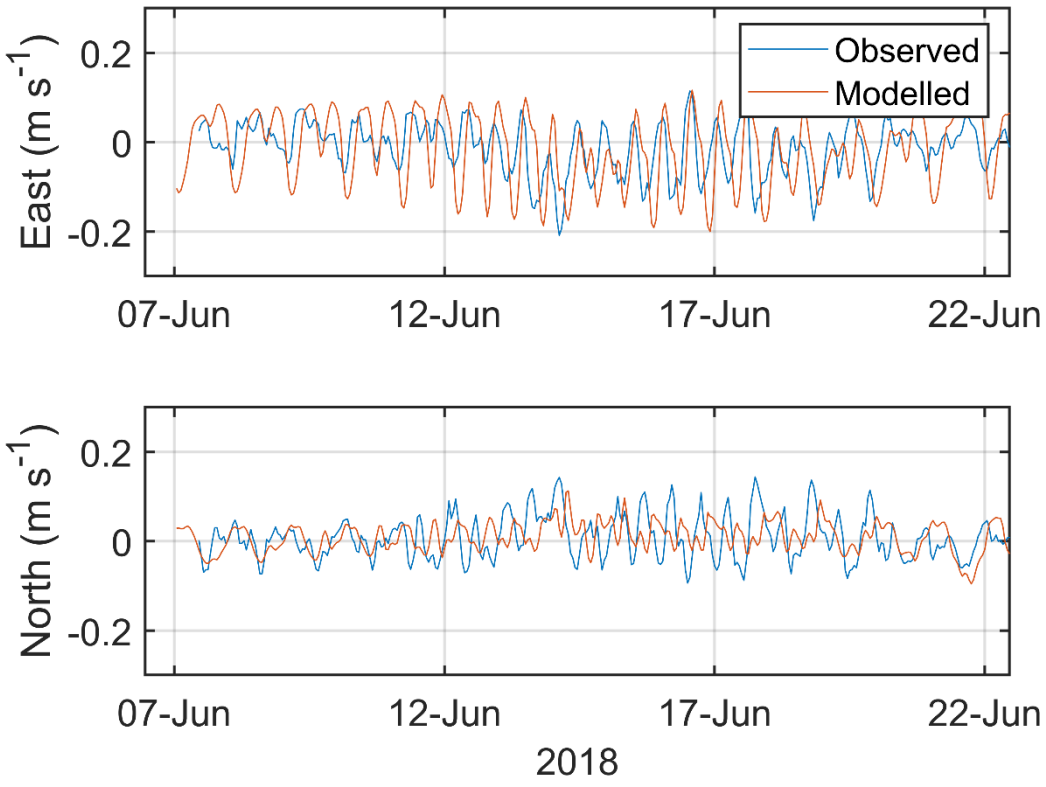

Figure 6. Comparison between observed and modelled East (top) and North (bottom) components of velocity at the ADCP location for 15 days in June - August 2018 (ID229). Observed data are in blue, model results in red.

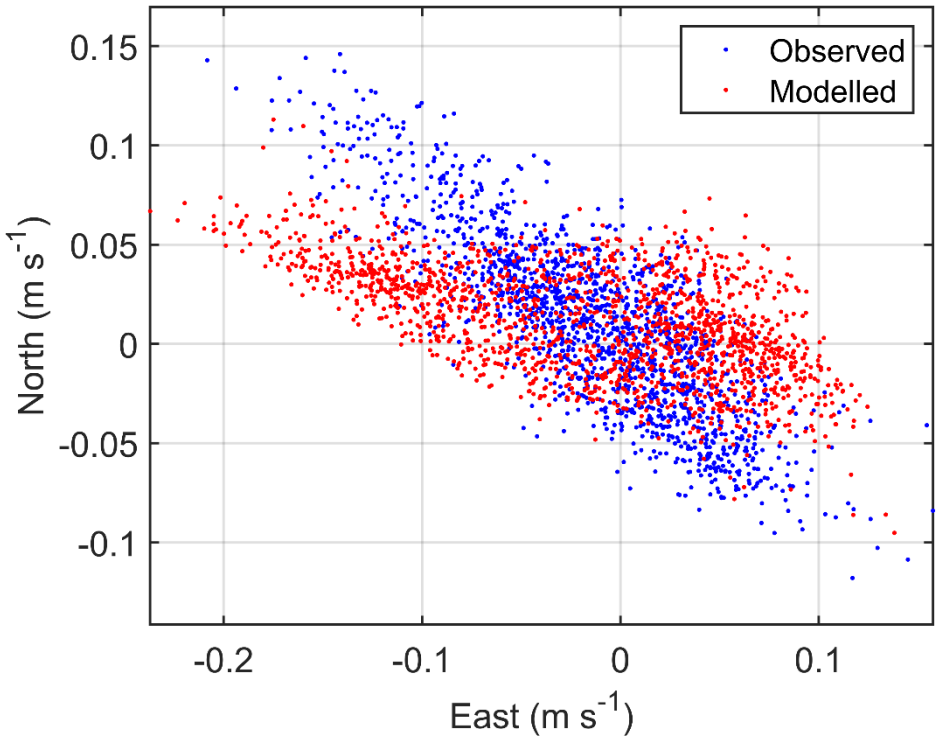

Figure 7. Scatter plot of observed and modelled velocity at the ADCP location from June – August 2018 (ID229). Observed data are in blue, model results in red.

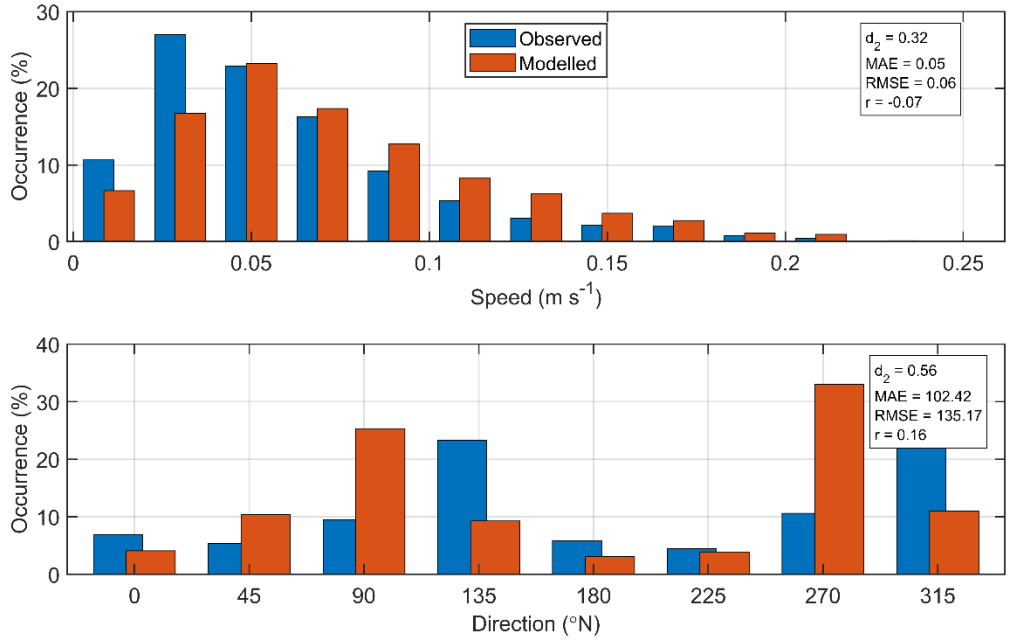

Figure 8. Histograms of observed and modelled speed (top) and direction (bottom) at the ADCP location from June – August 2018 (ID229). Observed data are in blue, model results in red.

3.2 Validation: August – October 2018, ID239

At the ADCP location, the sea surface height was reasonably accurately modelled, with model skill of 0.99 (Figure 9, Table 3). The mean absolute error (MAE) and root-mean-square error (RMSE) values of 0.18 m and 0.22 m are about 4.3% and 5.2 % of the spring tide range (4.2m) respectively.

East and North components of velocity at the ADCP location were satisfactorily reproduced by the model, with values of the model skill, d_2, of 0.55 and 0.35 respectively (Figure 10, Table 3). The values of the MAE and RMSE being in the range 5-9 cm s^{-1} (Table 3). The scatter plots and histograms shown in Figure 11 and Figure 12 demonstrate that the modelled currents were broadly of the same speed and direction as the observed data, although the offset between the orientation of the modelled and observed currents remains (Figure 11).

Table 3. Model performance statistics for sea surface height (SSH) and East and North velocity at the ADCP location from August – October 2018 (ID239).

	SSH	East	North
Skill, d_2	0.99	0.55	0.35
Mean Absolute Error (MAE)	0.18 m	0.07 m s^{-1}	0.05 m s^{-1}
Root-Mean-Square Error (RMSE)	0.22 m	0.09 m s^{-1}	0.07 m s^{-1}

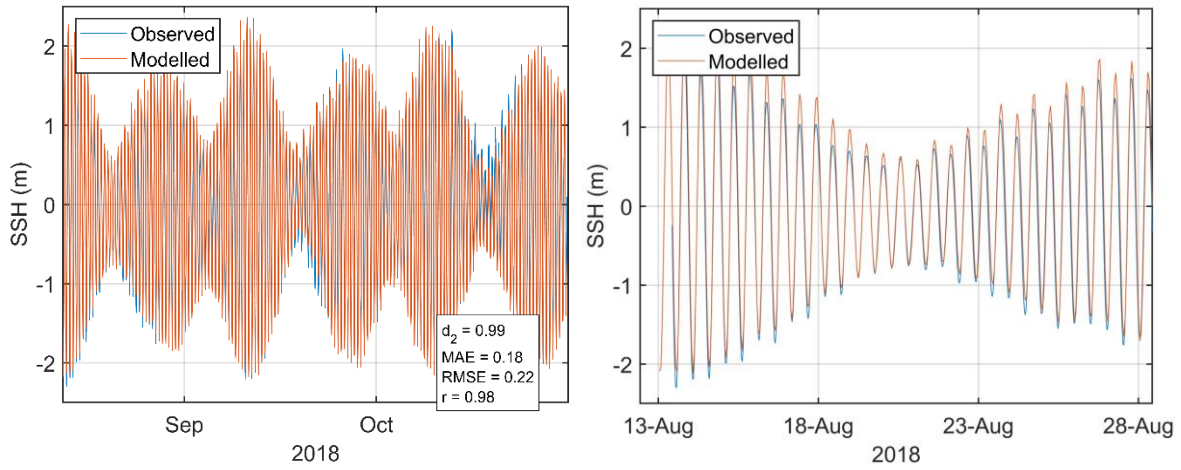

Figure 9. Comparison between observed and modelled sea surface height from August – October 2018 (ADCP deployment ID239) using model parameter values from Table 1. Both the full record (left) and a subset of 15 days (right) are shown. Observed data are in blue, model results in red.

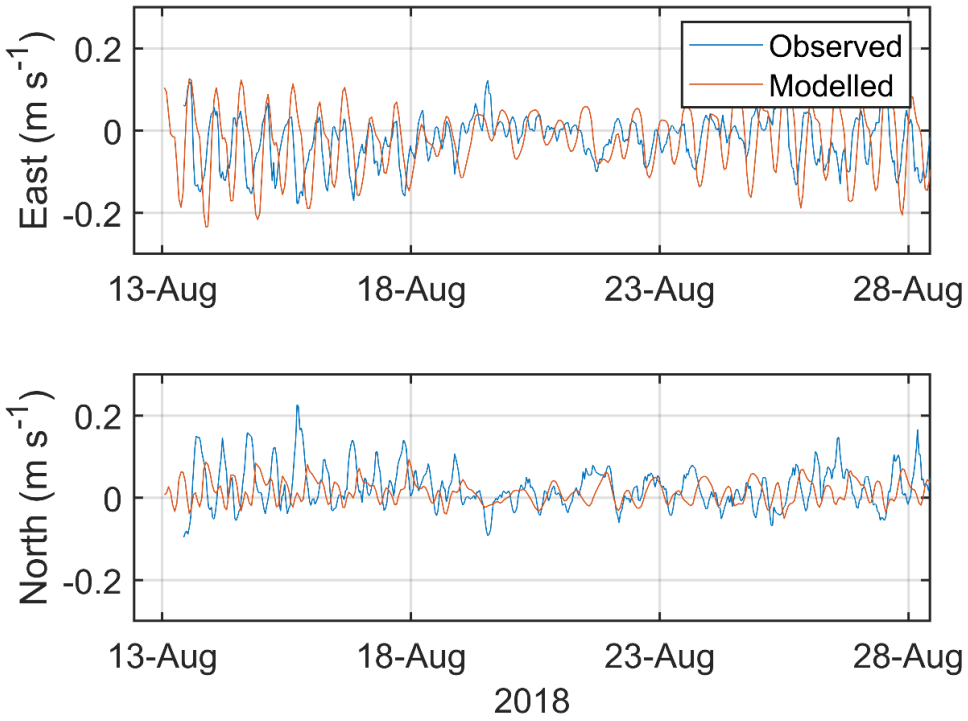

Figure 10. Comparison between observed and modelled East (top) and North (bottom) components of velocity at the ADCP location for 15 days in August – October 2018 (ID239). Observed data are in blue, model results in red.

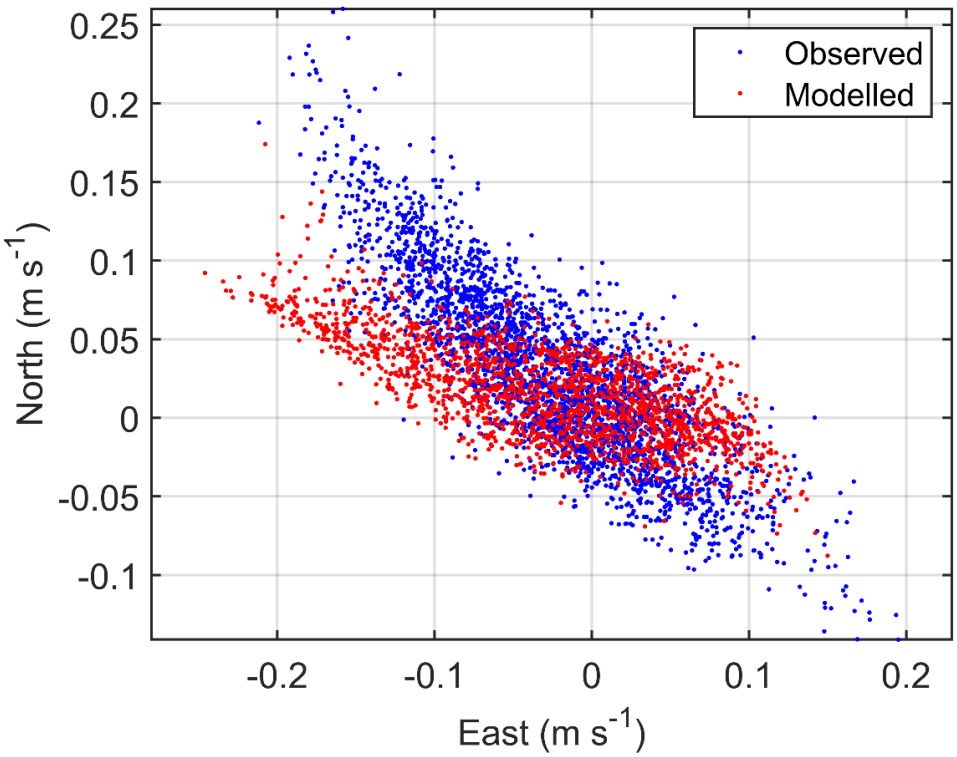

Figure 11. Scatter plot of observed and modelled velocity at the ADCP location from August – October 2018 (ID239). Observed data are in blue, model results in red.

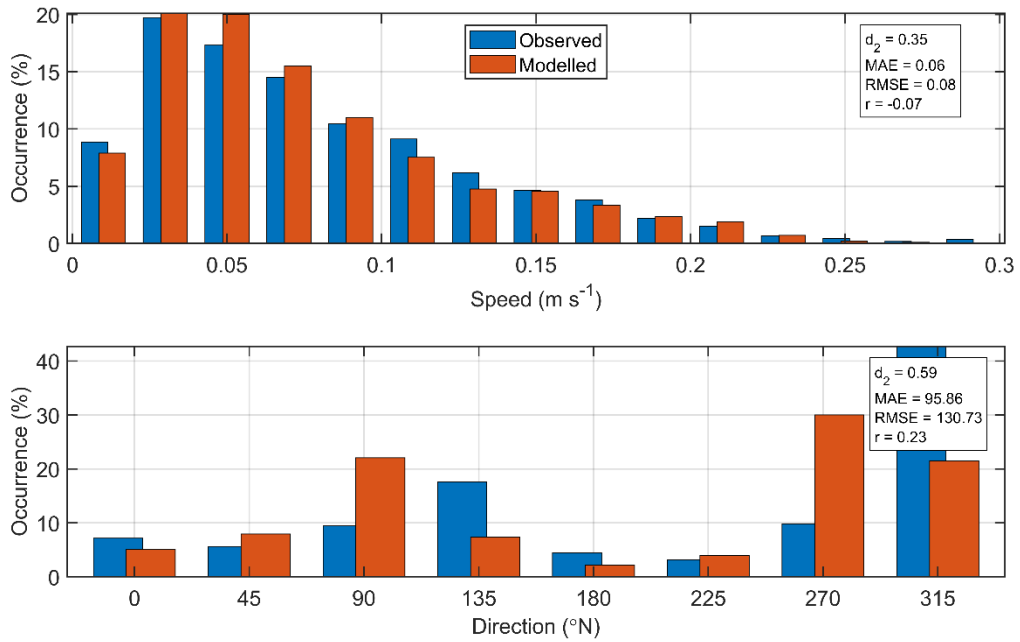

Figure 12. Histograms of observed and modelled current speed (top) and direction (bottom) at the ADCP location from August – October 2018 (ID239). Observed data are in blue, model results in red.

4. Modelled Flow Fields (ID239)

Modelled flood and ebb velocity vectors at spring tides are illustrated in Figure 13. The Hellisay site is exposed to strong currents from the Sea of the Hebrides, with flood tide current speeds of up to 20 – 25 cm s^{-1}. The prevailing flow is to the west-north-west, into the archipelago; deposited solids may be expected to be preferentially transported in this direction. Currents are moderate around the Hellisay site, with a mean near-surface speeds of 0.08 – 0.09 m s^{-1} and near-bed current speeds of 0.057 – 0.080 m s^{-1}.

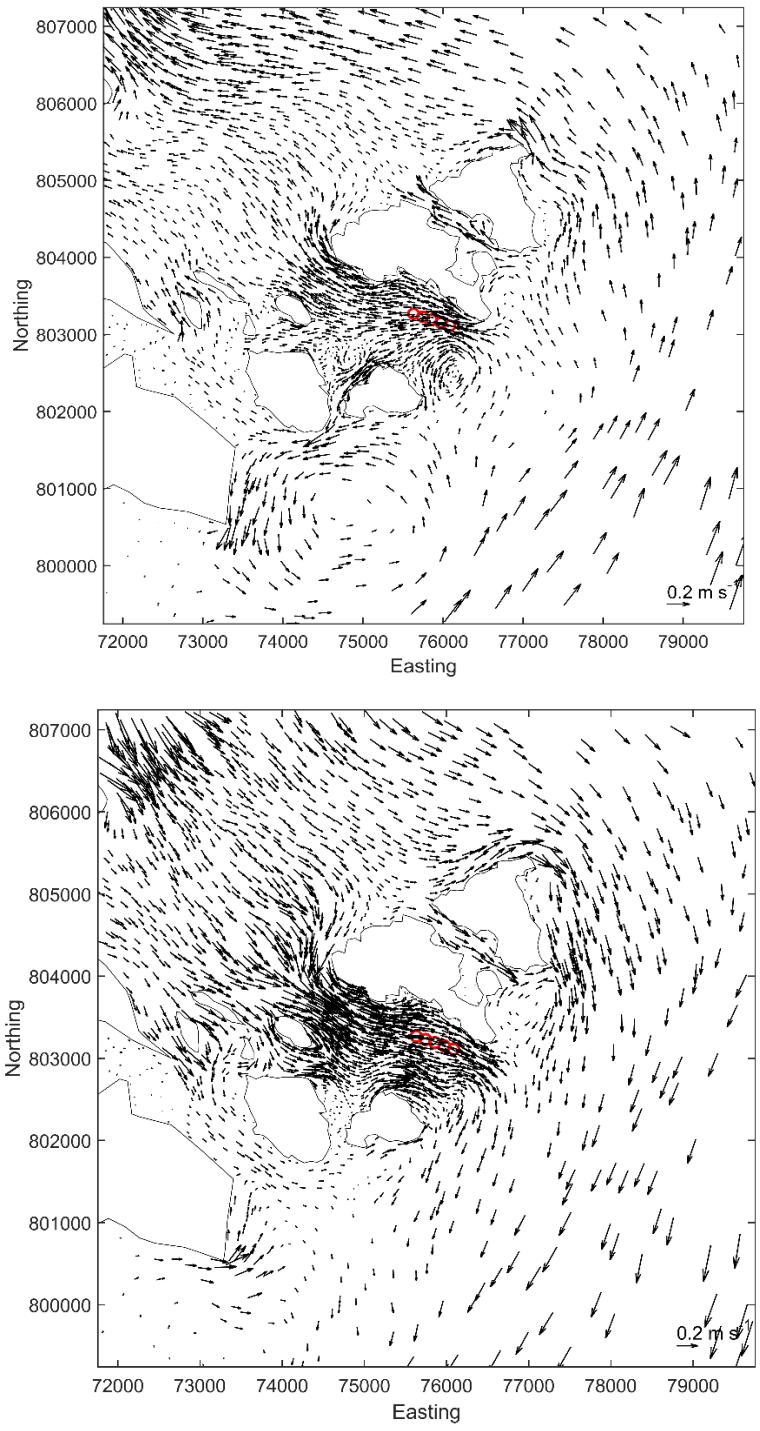

Figure 13. Modelled flood (top) and ebb (bottom) surface current vectors during spring tides. For clarity, only every 10th vector is shown.

5. References and Bibliography

Casulli, V. 1987. Eulerian-lagrangian methods for hyperbolic and convection dominated parabolic problems. In: Taylor, C., Owen, D., Hinton, E. (Eds.), Computational Methods for Non-linear Problems, Pineridge Press, Swansea,U.K., pp. 239–268.

European Centre for Medium-Range Weather Forecasts (ECMWF) 2021, ERA5 Dataset https://www.ecmwf.int/en/forecasts/datasets/reanalysis-datasets/era5

Gillibrand, P.A.; Lane, E.M.; Walters, R.A.; Gorman, R.M. 2011. Forecasting extreme sea surface height and coastal inundation from tides, surge and wave setup. Austr. J. Civil Eng. 9, 99-112.

Gillibrand, P.A., Walters, R.A., and McIlvenny, J., 2016. Numerical simulations of the effects of a tidal turbine array on near-bed velocity and local bed shear stress. *Energies*, vol 9, no. 10, pp. 852. DOI: 10.3390/en9100852

Lane, E.M.; Gillibrand, P.A.; Arnold, J.R.; Walters, R.A. 2011. Tsunami inundation modelling with RiCOM. Austr. J. Civil Eng., 9, 83-98.

Large. W.G. and Pond, S., 1981. Open ocean momentum flux measurements in moderate to strong winds. J. Phys. Oceanogr., 11, 324—336.

Marine Scotland, 2016. Scottish Shelf Model. Part 1: Shelf-Wide Domain. Available at http://marine.gov.scot/taxonomy/term/1964#:~:text=The%20Scottish%20Shelf%20Model%20%20%20%20,%20%20%20%2016%20more%20rows%20

McIlvenny, J. , Tamsett, D., Gillibrand, P.A. and Goddijn-Murphy, L., 2016. Sediment Dynamics in a Tidally Energetic Channel: The Inner Sound, Northern Scotland. Journal of Marine Science and Engineering, 4, 31; doi:10.3390/jmse4020031

Mowi Scotland Ltd, 2022. Hellisay Azamethiphos Dispersion Modelling Report. July 2022.

Plew, D. R.; Stevens, C. L. 2013. Numerical modelling of the effect of turbines on currents in a tidal channel–Tory Channel, New Zealand. Renew. Energy, 57, 269-282.

Walters, R. A. 2005a. Coastal ocean models: two useful finite element methods. Cont. Shelf Res., 25(7), 775-793.

Walters, R. A. 2005b. A semi-implicit finite element model for non-hydrostatic (dispersive) surface waves. Int. J. Num. Meth. Fluids, 49(7), 721-737.

Walters, R.A. 2016. A coastal ocean model with subgrid approximation. *Ocean Mod*., 102, 45-54.

Walters, R.A.; Casulli, V., 1998. A robust, finite element model for hydrostatic surface water flows. Comm. Num. Methods Eng., 14, 931–940.

Walters, R.A.; Gillibrand, P.A.; Bell, R.; Lane, E.M. 2010. A Study of Tides and Currents in Cook Strait, New Zealand. Ocean Dyn., 60, 1559-1580.

Walters, R.A., Lane, E.M., Hanert, E. 2009. Useful time-stepping methods for the Coriolis term in a shallow water model. *Ocean Model*., *28*, 66–74. doi: 10.1016/j. ocemod.20 08.10.0 04.

Walters, R.A. ; Lane, E.M.; Henry, R.F. 2008. Semi-lagrangian methods for a finite element coastal ocean model. *Ocean Model*., 19, 112–124.

Walters, R. A.; Tarbotton, M. R.; Hiles, C. E. 2013. Estimation of tidal power potential. Renew. Energy, 51, 255-262.

Willmott, C. J.; Ackleson, S. G.; Davis, R. E.; Feddema, J. J.; Klink, K. M.; Legates, D. R. O'Donnell, J.; Rowe, C. M. 1985. Statistics for evaluation and comparison of models, J. Geophys. Res., 90, 8995– 9005.

Wu, J. 1982. Wind-stress coefficients over sea surface from breeze to hurricane, J. Geophys. Res., 87(C12), 9704–9706, doi:10.1029/JC087iC12p09704.